LA-UR-77-1997

TITLE: NONLINEAR HYDRODYNAMIC FORCES ON FLOATING BODIES

AUTHOR(S): B. D. Nichols and C. W. Hirt

SUBMITTED TO: Second International Conference on
Numerical Ship Hydrodynamics
Berkeley, CA - 19-21 September 1977

los alamos
scientific laboratory
of the University of California
LOS ALAMOS, NEW MEXICO 87545

An Affirmative Action/Equal Opportunity Employer

NONLINEAR HYDRODYNAMIC FORCES IN FLOATING BODIES*

B. D. Nichols and C. W. Hirt
University of California
Los Alamos Scientific Laboratory
Los Alamos, New Mexico 87545

ABSTRACT

This study investigates the influence of [illegible]

[illegible]

INTRODUCTION

[illegible]

[illegible]

for completeness. Presented are also data from the triangular cylinder in forced roll motion. The added mass coefficient, [illegible] and the damping coefficient, [illegible] are given by

[illegible]

[illegible]

where [illegible] is the amplitude of motion, [illegible] is the amplitude of [illegible] pressure force on the [illegible] [illegible]

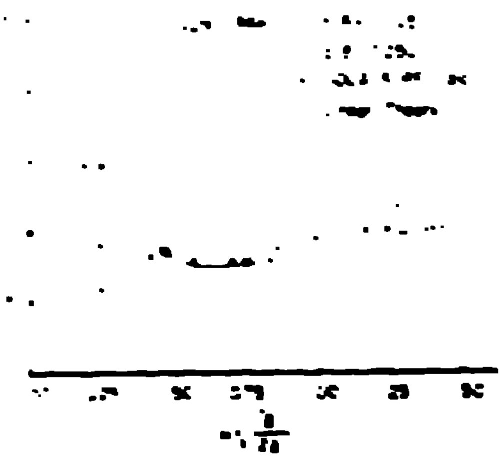

[illegible]

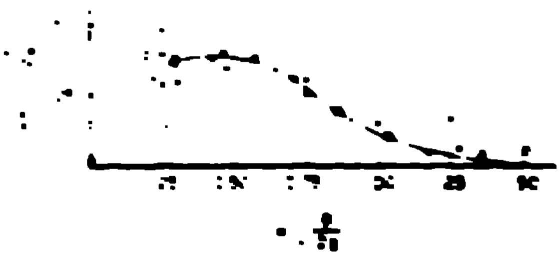

[illegible]

tangular cylinder and [illegible] = [illegible] for the triangular cylinder, where [illegible] is the initial draft of the cylinder. The amplitudes of motion, normalized by [illegible], for the rectangular cylinder were [illegible] and [illegible] and for sway was [illegible]. The triangular cylinder in roll motion rotated about an axis located at the horizontal center of the wedge and the initial free surface position. The amplitudes of motion were [illegible] and [illegible] radians.

In general, the numerical data from these calculations are in good agreement with linear theory. The sway (Fig. [illegible]) and roll (Fig. [illegible]) numerical data show some discrepancy with the experimental data, which is believed to result from elastic bending in the support bar used to hold the body in the experimental setup. Although there was secondary flow at the tip of the triangular cylinder in the sway and roll calculations, we found, as [illegible] suggested from his observation of these secondary vortices in his experiments, that this did not disturb the net pressure force over the cylinder surface. We believe these numerical experiments reconfirm the usefulness of linear, potential flow theory [illegible]

Large Amplitude Studies

[illegible]

[illegible]

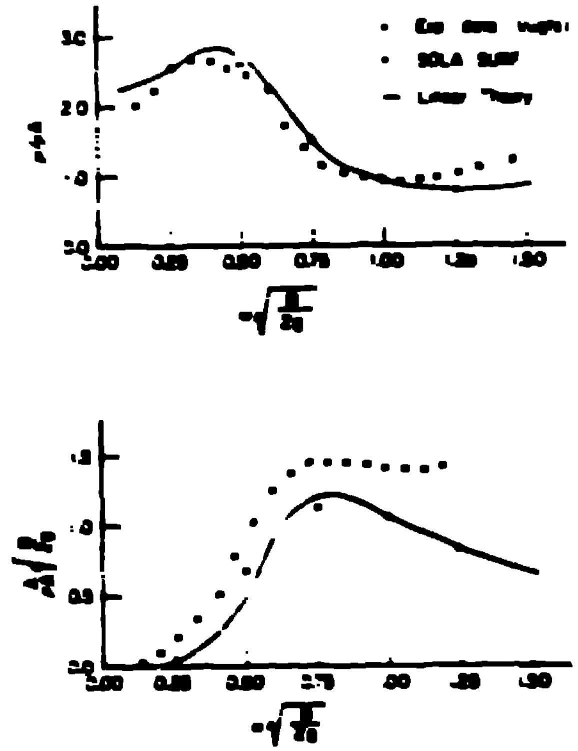
SOLA SURF
Linear Theory
0.00
0.25
0.50
0.75
1.00

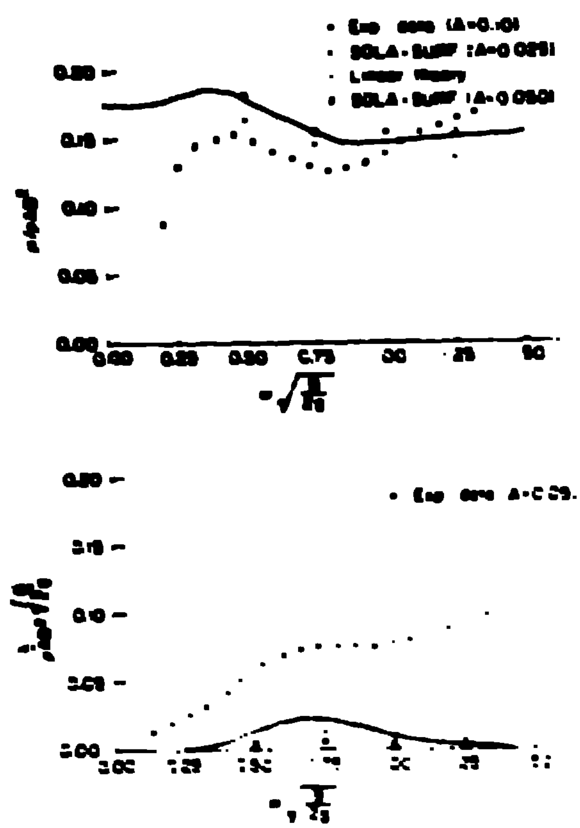
SOLA-SURF
Linear Theory
0.00
0.05
0.10
0.15
0.20

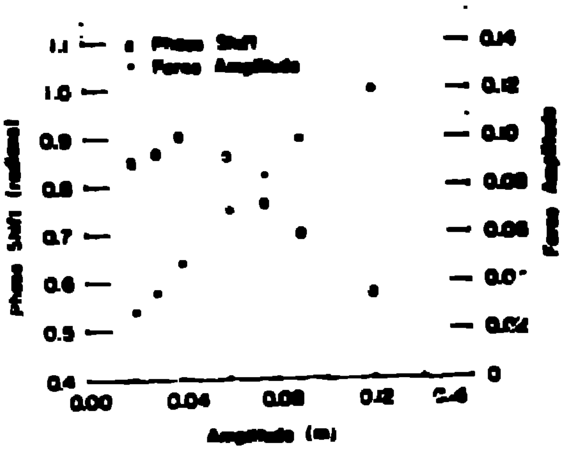

Fig. [ ]. Phase shift and amplitude of the dynamic pressure force as functions of the rectangular cylinder displacement amplitude.

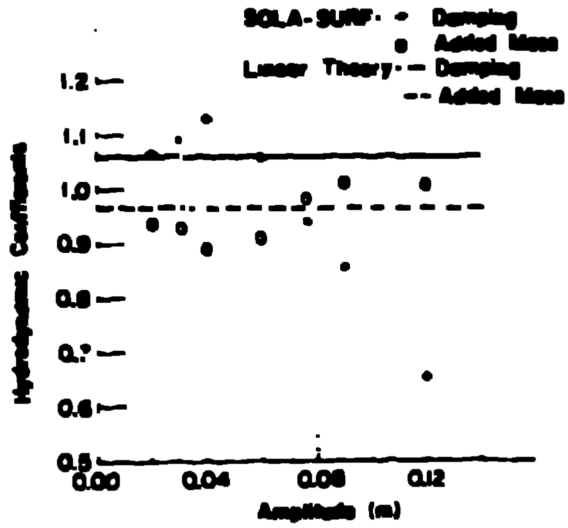

Fig. 5. Normalized added mass and damping coefficients as functions of the [ ] rectangular cylinder displacement amplitude.

[illegible] boundary conditions are needed for the [illegible] ... These conditions are derived under the constraint that the gas pressure at the free surface must equal the pressure outside the [illegible] ... [illegible] free surface boundary conditions are determined. [illegible]

[illegible]

case are compensated for by more negative downstream pressures. As a result, the net forces on the cylinder are nearly the same in the two cases. The eddies generated in the nonpotential case do not carry away kinetic energy because they are alternately generated and destroyed as the body moves to and fro.

III. NONLINEAR THREE-DIMENSIONAL EFFECTS

Nonlinear and finite length effects influencing the hydrodynamic forces on three-dimensional floating cylinders may be studied using the SOLA-3D code. We utilized this three-dimensional code to investigate the end effects and nonlinear finite amplitude effects associated with a finite length [illegible] rectangular cylinder in forced sway.

Finite Length

The parameters for these three-dimensional calculations were chosen for comparison with the two-dimensional calculations. Calculations were made with sway amplitudes of motion of [illegible] and [illegible] of the rectangular cylinder beam width, i.e., [illegible] m and [illegible] m, at the still water level. The cylinder draft was equal to 0.665 beam widths and the normalized frequency of motion was [illegible]. The cylinder length to draft ratio was varied from two to four. The resulting phase shift of the dynamic pressure force relative to the cylinder displacement phase, and the amplitude of the hydrodynamic force per unit length for the three-dimensional calculations were virtually the same as the two-dimensional calculations. This brief study suggests, therefore, that the end effects of the rectangular cylinder are not significant for the amplitudes of motion and for cylinder length to draft aspect ratios greater than two. Length to draft ratios less than two were not investigated.

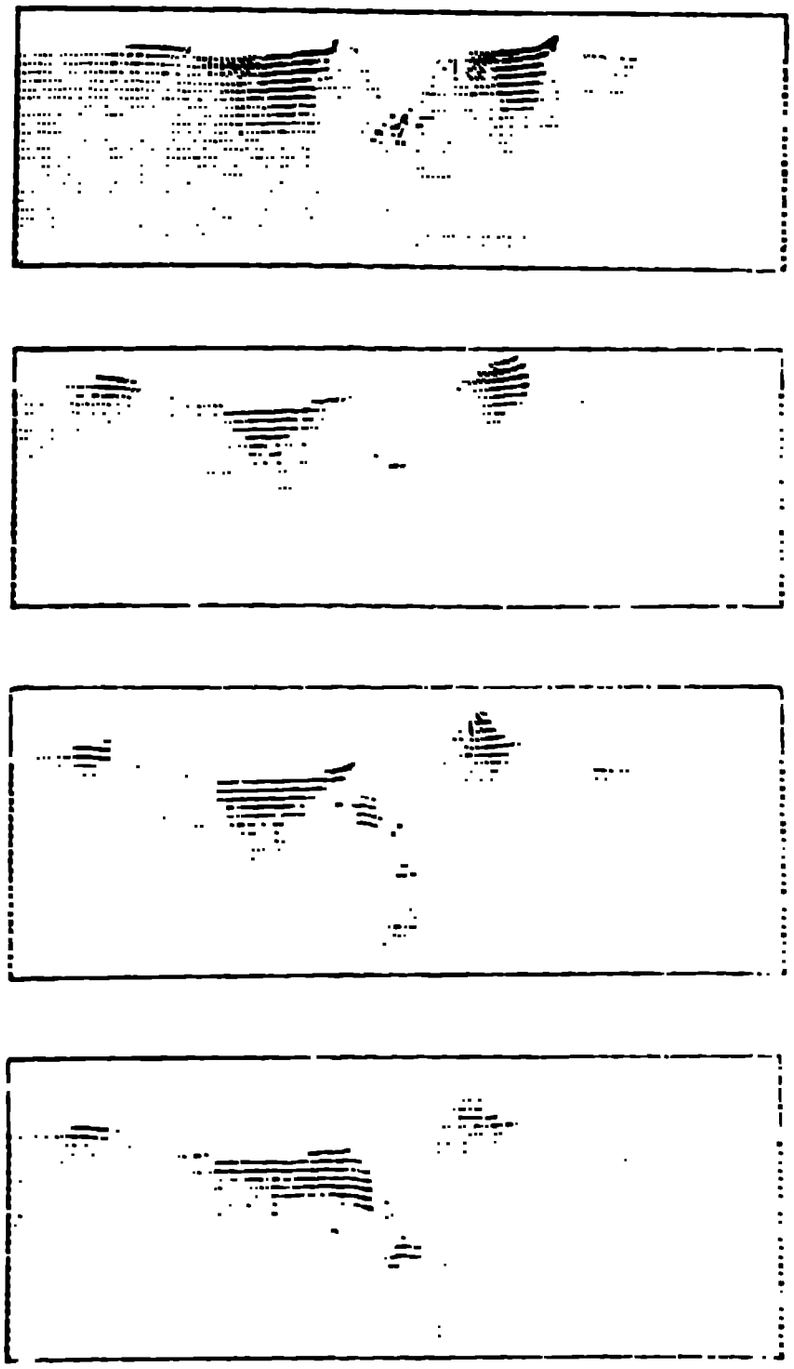

Fig. 6. [illegible]

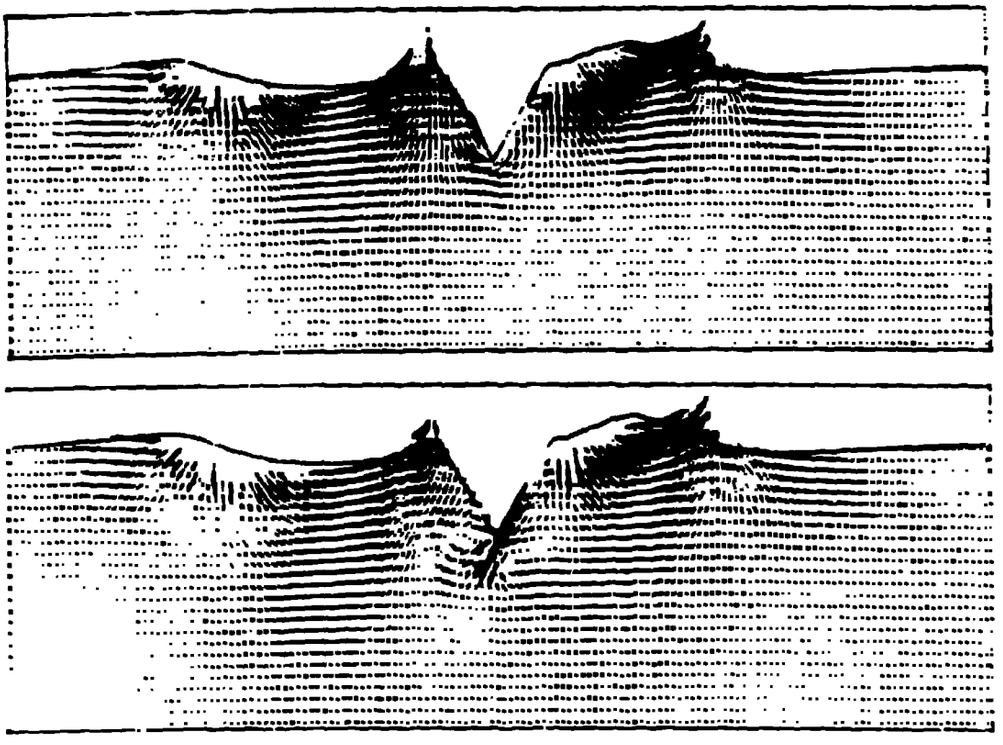

Fig. [illegible] Pressure profiles on a 60° triangular cylinder in sway determined from the SOLA-SURF code with and without the nonlinear potential flow option.

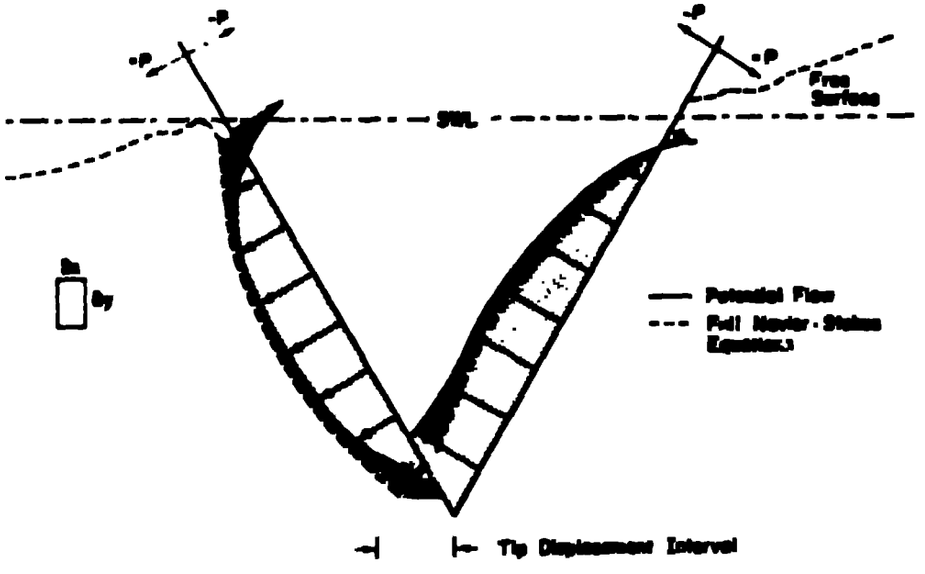

Fig. [illegible] Pressure profiles on a 60° triangular cylinder in sway determined from the SOLA-SURF code with and without the nonlinear potential flow option.

Typical velocity field plots for these low amplitude calculations are shown in Figs. 9 and 10. The entire velocity field in these planes is not shown, but only the region near the cylinder. Also, the magnification of the velocity vectors varies from plane to plane. Velocity fields in planes normal to the axis of the cylinder are shown in Fig. 9. The left velocity field is of the plane nearest the cylinder end and the right plot is of the velocity field in the plane immediately outside the cylinder end. At the time of these plots the cylinder is moving to the right after 2.11 periods of oscillation. The three-dimensional effect of the flow is clearly shown in the right plot. The larger velocity flow at the left (downstream) edge of the cylinder does not continue past the cylinder end in this plane, but flows around the edge. This is also clearly shown in the right plot of Fig. 10, which is of a horizontal plane near the vertical center of the cylinder. The fluid flows around the downstream side of the cylinder. The velocity field in the vertical plane through the center of the cylinder and parallel to its axis is shown in the left plot in Fig. 10. Secondary vortex flow is seen near the cylinder end in all the planes shown. However, as in the two-dimensional calculations, these vortices appear to have no significant influence on the net hydrodynamic forces on the body.

Large Amplitude

The most significant effect of the increase in amplitude in the two-dimensional calculations, as discussed above, was a significant decrease in the phase shift of the dynamic pressure force relative to the cylinder displacement phase. The force amplitude increased linearly with the cylinder displacement amplitude. We made corresponding large amplitude, three-dimensional calculations to compare with the two-dimensional study.

The three-dimensional calculations were for amplitudes of motion from 0.058 to 0.216 of the beam width, i.e., .020 m to 0.075 m. (At larger amplitudes the free surface slope near the cylinder end violated the code requirement that the slope not be greater than the slope of the cell diagonal.) The draft of the 60° triangular cylinder was 0.365 beam widths and the length to draft aspect ratio was two. As in the two-dimensional case, the force amplitude increased linearly as the cylinder displacement amplitude increased (see Fig. 11). However, as seen in Fig. 12, the decrease in the phase shift of the dynamic pressure force relative to the cylinder displacement phase observed in the two-dimensional case was not observed in these finite-length calculations. The phase shift is less for all amplitudes of motion but does not decrease significantly as the amplitude increases. It is possible, however, that at still larger amplitudes of motion the phase shift would show a decrease.

The added mass and damping coefficients determined from these three-dimensional calculations are compared with the two-dimensional SOLA-SURF data and linear theory in Figs. 13 and 14. In keeping with the two-dimensional data, the added mass coefficients are within a few per cent of the linear theory. The damping coefficient, again, follows the trend in the phase shift.

We earlier noted that in the infinite length case the phase shift decreased as the body velocity increased (i.e., at larger amplitudes of motion at a set frequency) because the fluid closest further downstream on the sides of the body and caused the force on the cylinder to be more in phase with the body, i.e., the phase shift was reduced. The probable reason for the phase shift not decreasing in the finite length case is that in the

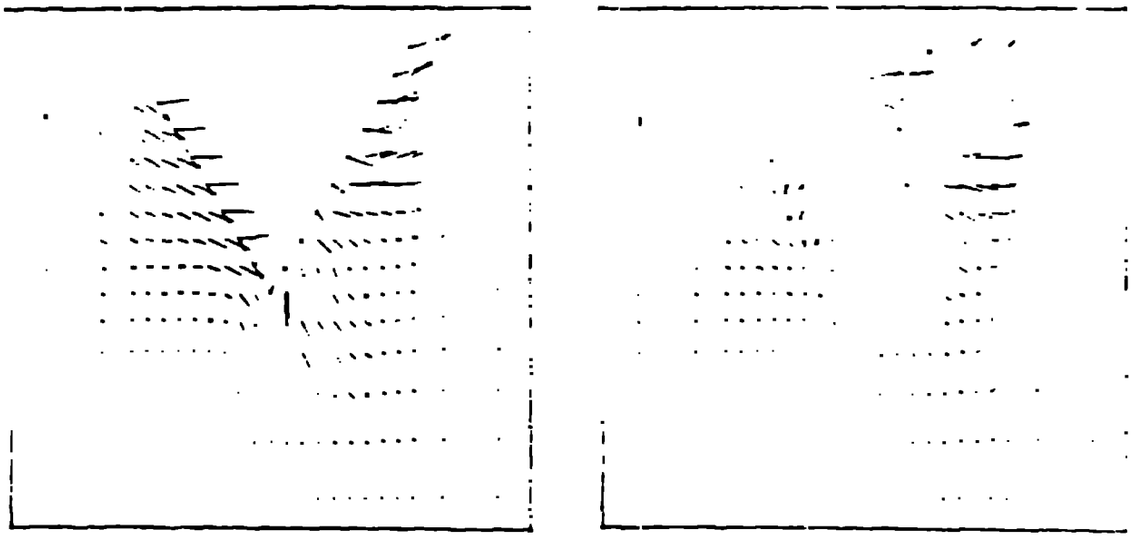

Fig. 9. Local velocities in planes normal to the axis of the three-dimensional triangular cylinder in low amplitude motion after 2.11 periods. The left plot is the plane nearest the cylinder end and the right plot is the plane immediately outside the cylinder end.

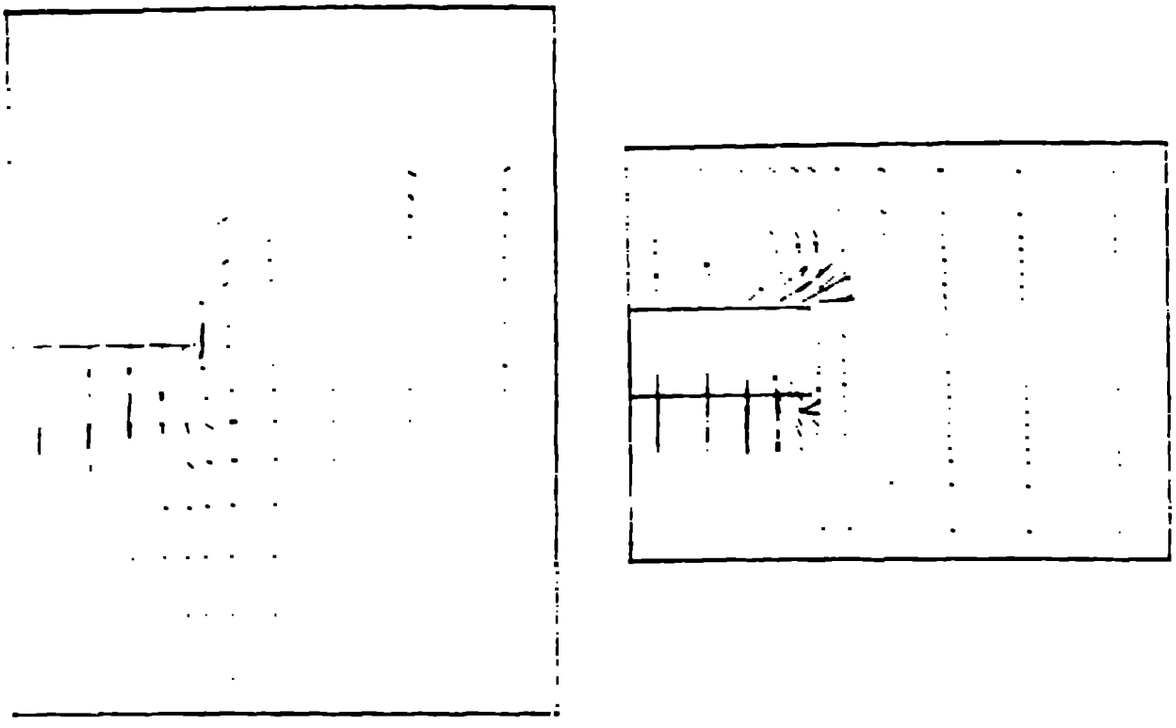

...velocities in a vertical plane through the center of the cylinder and parallel to its axis (left) and in a horizontal plane near the vertical center of the cylinder (right) after two periods.

...ampitudes of motion fluid flows freely around the cylinder end and does not build up at the ...ates.

The flow pattern around the cylinder for the ... amplitudes reinforces this interpre... Figures 15 and 16 show the velocity ... near the cylinder for an amplitude of ... (1.06 m) after two periods of ... Again, the magnification of the velocity vectors is different for each of the ... Velocity fields in planes normal to the axis of the cylinder are shown in Fig. 15. The left velocity vector plot is of the plane ...rough the cylinder end. As observed in Fig. ... the two-dimensional case, very strong ... vortex flow is formed near the tip of the cylinder. The right plot in Fig. 15 is of ... plane immediately outside the cylinder end. ... the time of these plots the cylinder has reached the leftmost point of its displacement after two periods of oscillation. The left plot in Fig. 16 is of the velocity field in the ...vertical plane through the center of the cylinder and parallel to its axis. This shows the downward motion of the fluid at the end of the ...linder, resulting in the small vortex off the ...linder end. The right plot in Fig. 16 shows the secondary flow on the downstream side of the cylinder in the horizontal plane near the ...vertical center of the cylinder. These velocity fields at selected planes show the flow ...und the ...linder end and downward flow near the end for this time. The resulting free surface configuration is shown in Fig. 17.

IV. CIRCULAR CYLINDER IMPACT

The SOLA-SURF code was used to calculate the force of impact on a circular cylinder during constant velocity entry into a pool of water. The cylinder boundary was approximated by straight line segments. The rigid-fluid interface boundary condition applied to each line segment was successfully used for determining the hydrodynamic forces on the rectangular and triangular cylinders in forced motion discussed above. Specifically, at the rigid-fluid interface the cell pressure is derived from the constraint that the normal fluid velocity be equal to that of the cylinder. As a free fluid surface approaches a rigid boundary, a simple linear combination of the rigid and free boundary condition is used. This is needed to eliminate the sudden transition in boundary conditions, which may result in excessively large pressure spikes. For partially submerged bodies moving at relatively small velocities, this ad hoc linear combination of boundary conditions worked very well. For the impact problems, however, a modification was necessary because the fluid did not anticipate the presence of the rigid boundary in sufficient time before impact and the calculation consequently exhibited unacceptably large pressure oscillations. Through a heuristic argument based on the need

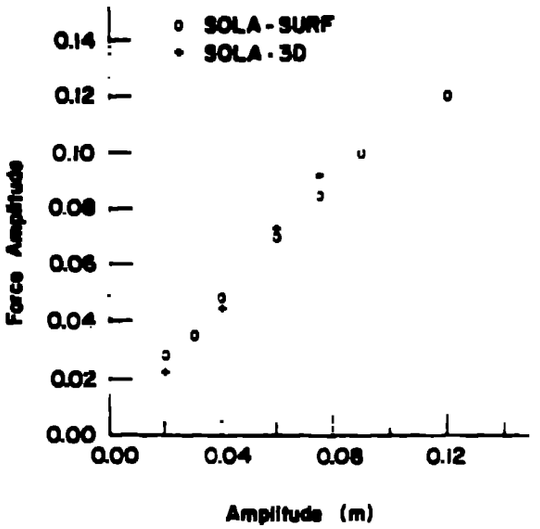

Fig. 11. Amplitude of the dynamic pressure force as a function of cylinder displacement amplitude.

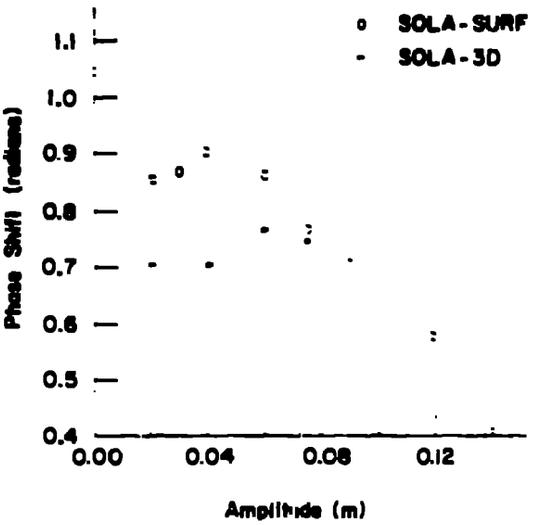

Fig. 12. Phase shift of the dynamic pressure force relative to the cylinder displacement phase as a function of the cylinder displacement amplitude.

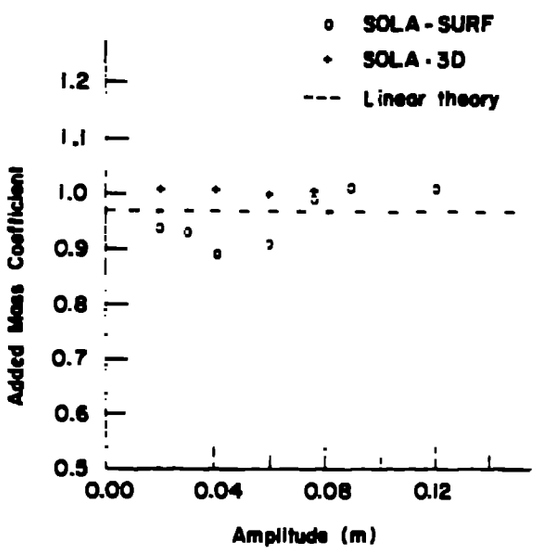

Fig. 13. Normalized added mass coefficient as a function of the cylinder displacement amplitude.

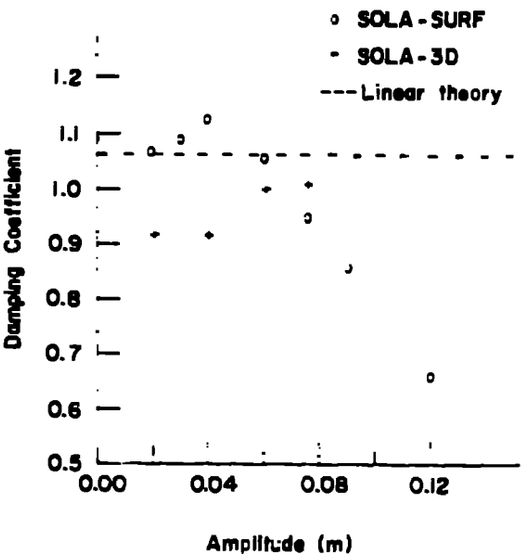

Fig. 14. Normalized damping coefficient as a function of the cylinder displacement amplitude.

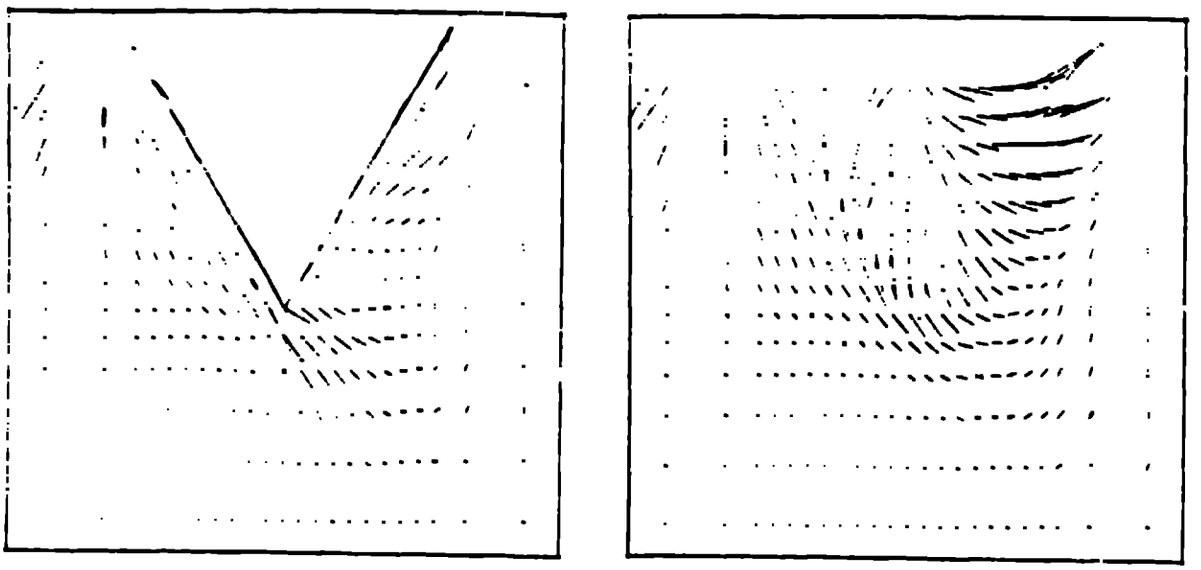

Fig. 15. Local velocities in planes normal to the axis of the triangular cylinder in large amplitude motion after 2.0 periods. The left plot is the plane nearest the cylinder end and the right plot is the plane immediately outside the cylinder end.

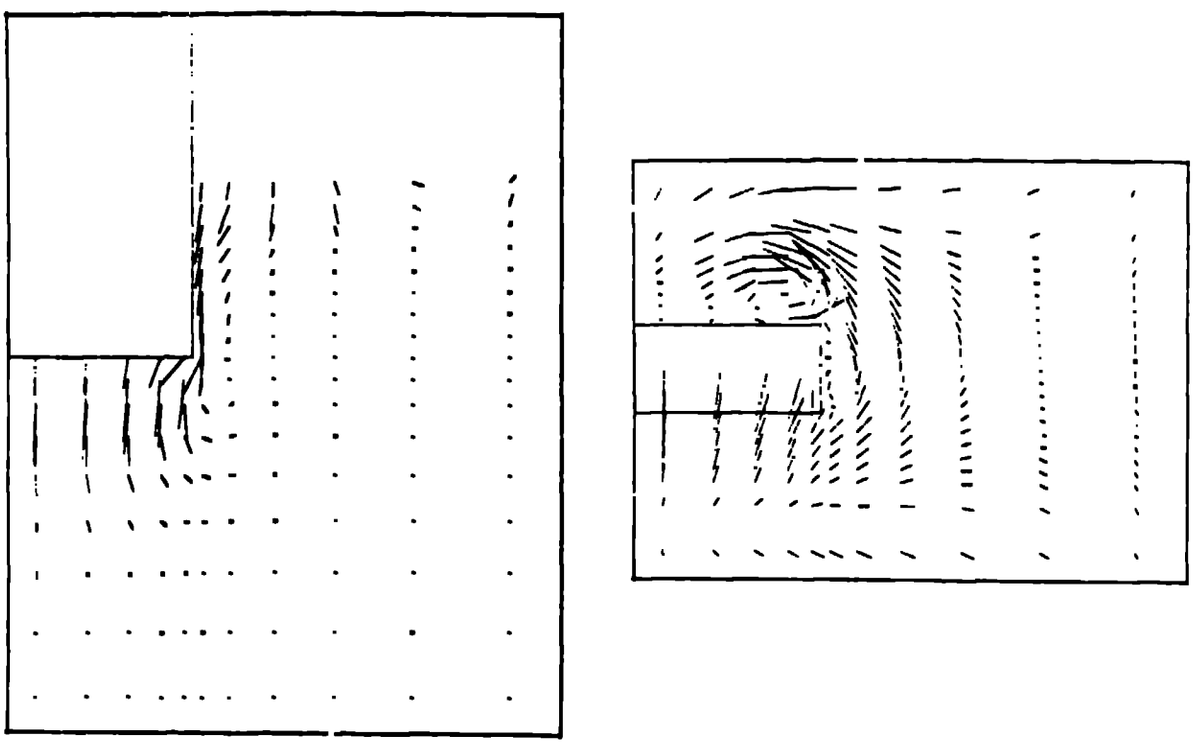

Fig. 16. Local velocities in a vertical plane through the center of the cylinder and parallel to its axis (left) and in a horizontal plane near the vertical center of the cylinder (right) after 2.0 periods.

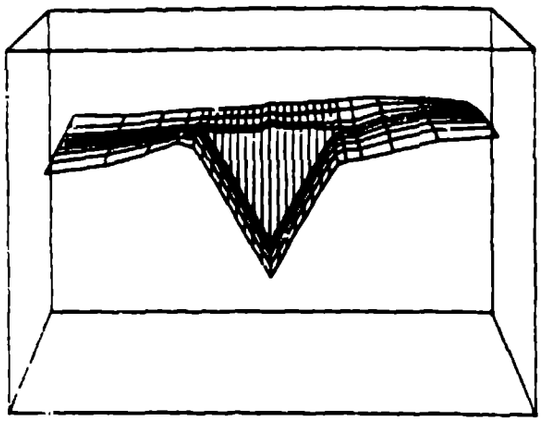

Fig. 17. Local free surface configuration resulting from the triangular cylinder in sway motion after 2.0 periods.

for an applied pressure on the fluid just sufficient to bring the normal component of the fluid and body velocities into agreement at the time of impact. a boundary condition combination was derived that did force a smooth transition between the free and rigid boundary conditions. The new combination uses a quadratic in the relative velocity term instead of the linear term used in the earlier ad hoc expression.

The average pressure on the cylinder, i.e., the vertical force per unit length divided by the cylinder diameter. was determined for a cylinder with a diameter of 8.25 inches and an impact velocity of 7.70 ft/sec. The calculation was run to a time of 18.0 msec. At this time the fluid has reached nearly 90° around the cylinder. Velocity vector plots in Fig. 18 show the velocity field with the free surface and the cylinder boundary at -7.85, 2.48, .0.75 and 18.00 msec. Because the calculation starts some time before the cylinder hits the surface, we shifted the calculated time scale so that the computed and measured peak forces occur at the same time.

A comparison of the numerically calculated average pressure and the experimental data[9] is shown in Fig. 19. (The experimental data is for an impact velocity of 7.65 ft/sec. and the computed data have been scaled from 7.70 ft/sec. to 7.65 ft/sec. for this comparison.) The experiment only had pressure transducers located along a portion of the lower surface of the cylinder. When the cylinder was wetted beyond the highest pressure gauge location the total force was estimated in two ways. In the first. extrapolation was used to estimate the unmeasured surface pressures and resulted in the upper of the two experimental curves appearing in Fig. 19 after t=3.0 msec. The lower curve is the result obtained using only the measured data and ignoring the pressures in the uninstrumented region. The agreement between the computed results and the upper experimental curve is excellent, except for some small, high frequency pressure oscillations around 6 msec. These oscillations are remnants of the discretization fluctuations that are not completely eliminated by the improved boundary condition combination discussed above.

V. CONCLUSIONS

Most ship hydrodynamic problems are solved by linear potential flow methods. Some limits of this approximate theory have been demonstrated by comparisons of calculated results using the SOLA-SURF code for the full, nonlinear Navier-Stokes equations with linear theory and the experimental data of Vugts. An essential assumption made in the linear theory is that the amplitude of motion be small with respect to the dimensions of the cylinder. Indeed, when this is no longer the case, nonlinear effects, as shown by the SOLA-SURF code, can be significant.

Three-dimensional, finite length effects were determined not to be significant for cylinders with either low or relatively high amplitudes of motion. Apparently the flow around the cylinder ends, for the short cylinders studied, minimizes the pile up of fluid at the fore and aft cylinder surfaces, which caused the large amplitude effect in the case of infinitely long cylinders.

The calculations of the cylinder impacting onto the free surface forced a needed improvement of the transition from free to rigid surface boundary conditions. It also served to further validate the SOLA-SURF code as a useful tool for calculating nonlinear fluid flow problems.

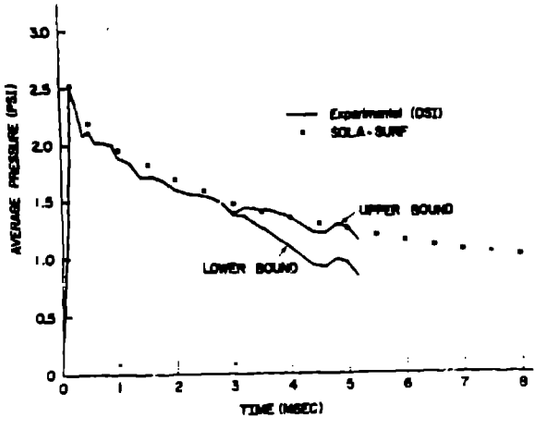

Fig. 19. Comparison of numerically computed and experimental data for the average pressure per unit length on an 8.25 in. diameter cylinder impacting with a constant velocity of 7.65 ft/sec.

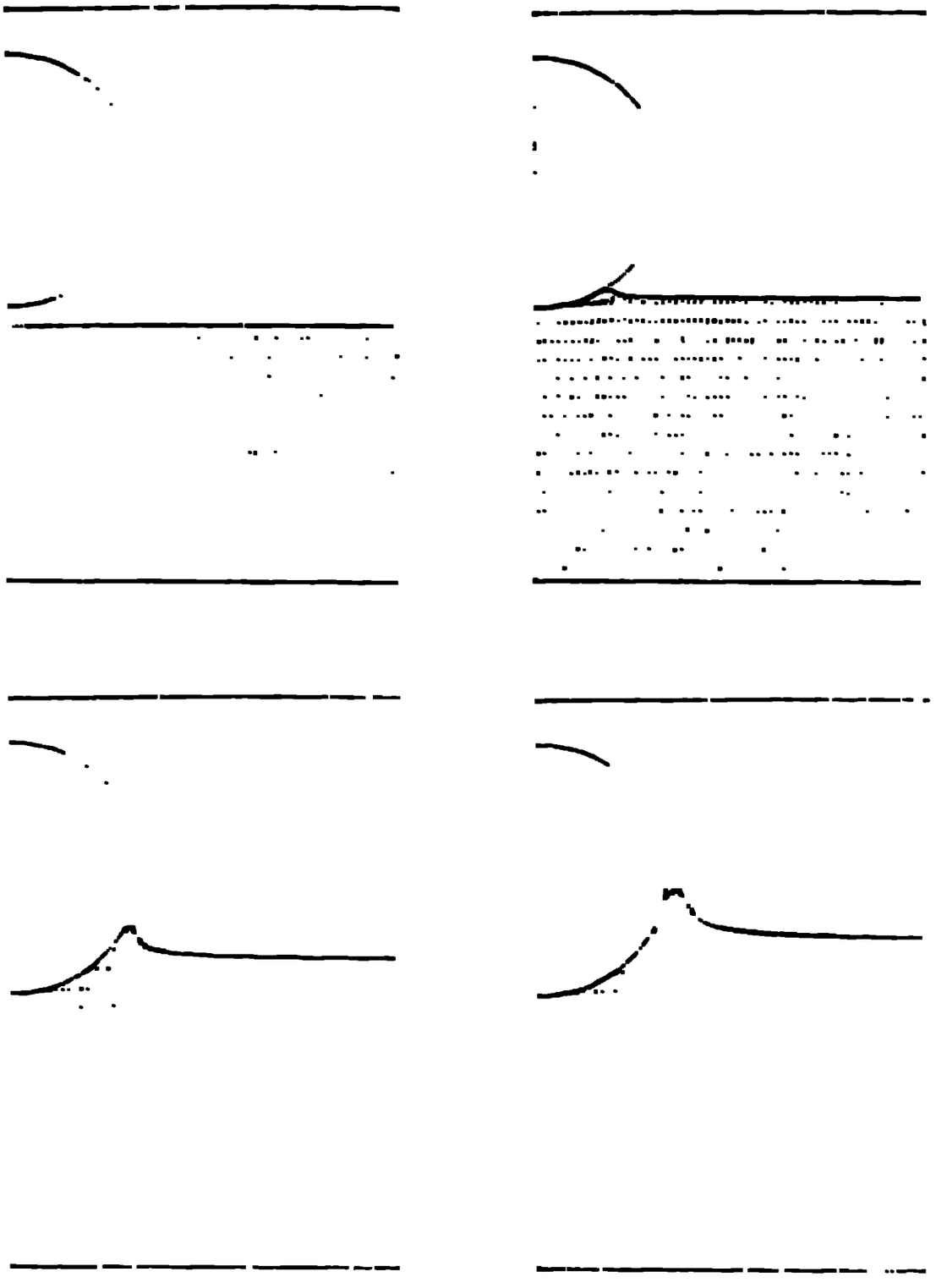

Fig. 10 Velocity vector plots showing the velocity field near the reactive cylinder when the free surface and cylinder bore at -0.05, 0.48, 0.75, and 1.0 sec.

ACKNOWLEDGMENTS

The authors wish to express their appreciation to Leland Stein for writing the SOLA-3D code and for many valuable suggestions in running the three-dimensional problems and to Juanita Salazar for so ably composing the text and figures of this paper.

REFERENCES

1. C. W. Hirt, B. D. Nichols, and N. C. Romero, "SOLA - A Numerical Solution Algorithm for Transient Fluid Flows," Los Alamos Scientific Laboratory report LA-5852 (April 1975); LA-5852, Addendum (January 1976).

2. B. D. Nichols and C. W. Hirt, "Methods for Calculating Multi-Dimensional, Transient Free Surface Flows Past Bodies," Proc. of the First Intern. Conf. on Numerical Ship Hydrodynamics, Gaithersburg, MD (1975).

3. B. D. Nichols and C. W. Hirt, "Numerical Calculation of Wave Forces on Structures," Proc. of the Fifteenth Intern. Conf. on Coastal Engineering, Honolulu, HI (1976).

4. B. D. Nichols and C. W. Hirt, unpublished work performed for the Office of Naval Research under contract N00014-75-C-0455.

5. C. W. Hirt and J. E. Ramshaw, "Prospects for Numerical Simulation of Stuff Body Aerodynamics," Proc. of the Aerodynamic Drag Mechanisms Symposium presented at General Motors Research Laboratories, Warren, MI (1976).

6. [illegible] Wehausen, "The Motion of Floating Bodies," Annual Review of Fluid Mechanics, [illegible] (1971).

7. C. W. Hirt, "The Hydrodynamic Coefficients for Heaving, Heaving, and Rolling Cylinders in a Free Surface," International Shipbuilding Progress, [illegible] (1972).

8. John J. Jones, Electric Power Research Institute Development Services, [illegible] private communication (1977).